Quantifying the contribution of thermally driven recirculation to a high-ozone event along the Colorado Front Range using lidar

John T. Sullivan, Thomas J. McGee, Andrew O. Langford, Raul J. Alvarez, Christoph J. Senff, Patrick J. Reddy, Anne M. Thompson, Laurence W. Twigg, Grant K. Sumnicht, Pius Lee, Andrew Weinheimer, Christoph Knote, Russell W. Long, Raymond M. Hoff

Angaben zur Veröffentlichung / Publication details:

Sullivan, John T., Thomas J. McGee, Andrew O. Langford, Raul J. Alvarez, Christoph J. Senff, Patrick J. Reddy, Anne M. Thompson, et al. 2016. "Quantifying the contribution of thermally driven recirculation to a high-ozone event along the Colorado Front Range using lidar." *Journal of Geophysical Research: Atmospheres* 121 (17): 10377–90. https://doi.org/10.1002/2016jd025229.

AGU PUBLICATIONS

JGR

Journal of Geophysical Research: Atmospheres

RESEARCH ARTICLE
10.1002/2016JD025229

Key Points:
- Thermally driven mountain-plains circulation and polluted return flow aloft exacerbated poor air quality in Colorado's Front Range
- Ozone and wind observations are utilized to provide a high-resolution characterization of the air quality episode
- Simulations further suggest the downward transport of ozone to sites within the Front Range

Correspondence to:
J. T. Sullivan,
john.t.sullivan@nasa.gov

Citation:
Sullivan, J. T., et al. (2016), Quantifying the contribution of thermally driven recirculation to a high-ozone event along the Colorado Front Range using lidar, *J. Geophys. Res. Atmos.*, *121*, 10,377–10,390, doi:10.1002/2016JD025229.

Received 13 APR 2016
Accepted 19 AUG 2016
Accepted article online 23 AUG 2016
Published online 15 SEP 2016

Quantifying the contribution of thermally driven recirculation to a high-ozone event along the Colorado Front Range using lidar

John T. Sullivan[1], Thomas J. McGee[1], Andrew O. Langford[2], Raul J. Alvarez II[2], Christoph J. Senff[3], Patrick J. Reddy[4], Anne M. Thompson[5], Laurence W. Twigg[6], Grant K. Sumnicht[6], Pius Lee[7], Andrew Weinheimer[8], Christoph Knote[9], Russell W. Long[10], and Raymond M. Hoff[11,12]

[1]Atmospheric Chemistry and Dynamics Laboratory, NASA Goddard Space Flight Center, Greenbelt, Maryland, USA, [2]NOAA Earth System Research Laboratory, Boulder, Colorado, USA, [3]Cooperative Institute for Research in Environmental Sciences, University of Colorado and NOAA Earth System Research Laboratory, Boulder, Colorado, USA, [4]National Center for Atmospheric Research, Boulder, Colorado, USA, [5]Earth Sciences Division, NASA Goddard Space Flight Center, Greenbelt, Maryland, USA, [6]Science Systems and Applications Inc., Lanham, Maryland, USA, [7]NOAA Air Resources Laboratory, NOAA Center for Weather and Climate Prediction, College Park, Maryland, USA, [8]Atmospheric Chemistry Observations and Modeling Laboratory, National Center for Atmospheric Research, Boulder, Colorado, USA, [9]Meteorologisches Institut, Ludwig-Maximilians-Universität München, Munich, Germany, [10]Office of Research and Development, U.S. Environmental Protection Agency, Research Triangle Park, North Carolina, USA, [11]Joint Center for Earth Systems Technology, Baltimore, Maryland, USA, [12]Department of Atmospheric Physics, University of Maryland, Baltimore County, Baltimore, Maryland, USA

Abstract A high-ozone (O_3) pollution episode was observed on 22 July 2014 during the concurrent "Deriving Information on Surface Conditions from Column and Vertically Resolved Observations Relevant to Air Quality" (DISCOVER-AQ) and "Front Range Air Pollution and Photochemistry Experiment" (FRAPPE) campaigns in northern Colorado. Surface O_3 monitors at three regulatory sites exceeded the Environmental Protection Agency (EPA) 2008 National Ambient Air Quality Standard (NAAQS) daily maximum 8 h average (MDA8) of 75 ppbv. To further characterize the polluted air mass and assess transport throughout the event, measurements are presented from O_3 and wind profilers, O_3-sondes, aircraft, and surface-monitoring sites. Observations indicate that thermally driven upslope flow was established throughout the Colorado Front Range during the pollution episode. As the thermally driven flow persisted throughout the day, O_3 concentrations increased and affected high-elevation Rocky Mountain sites. These observations, coupled with modeling analyses, demonstrate a westerly return flow of polluted air aloft, indicating that the mountain-plains solenoid circulation was established and impacted surface conditions within the Front Range.

1. Introduction

The combination of rapid population growth and diverse emissions sources within the complex terrain along the Front Range of the Colorado Rocky Mountains has led to significant ozone (O_3) pollution episodes both within the urban corridor [*Pétron et al.*, 2012] and at high-elevation mountain sites [*Benedict et al.*, 2013]. The U.S. Environmental Protection Agency (EPA) has accordingly designated the Denver-Boulder-Greeley-Fort Collins-Loveland Area (hereafter the Denver metropolitan area/North Front Range or DNFR) a moderate non-attainment area for ozone. This classification is calculated from a design value based on the 3 year running average (2012–2014) of the annual fourth highest maximum daily 8 h average (MDA8) surface mixing ratio. Design values greater than or equal to 76 parts per billion by volume (ppbv) are in violation of the standard [https://www3.epa.gov/airquality/greenbook/]. Importantly, the DNFR design value has been well in excess of both the 2008 National Ambient Air Quality Standards (NAAQS) of 75 ppbv and the revised 2015 NAAQS of 70 ppbv [*U.S. Environmental Protection Agency* (*EPA*), 2015a].

Persistent high-pressure systems and weak synoptic forcing often lead to stagnant conditions and poor air quality along the Colorado Front Range during summer with the local transport dominated by diurnally varying thermal flows [*Toth and Johnson*, 1985]. A conceptual diagram of one local transport phenomenon, the mountain-plains solenoid circulation, is presented in Figure 1 as observed on 22 July 2014 (accompanied by a complete ground monitoring site description in Figure 2).

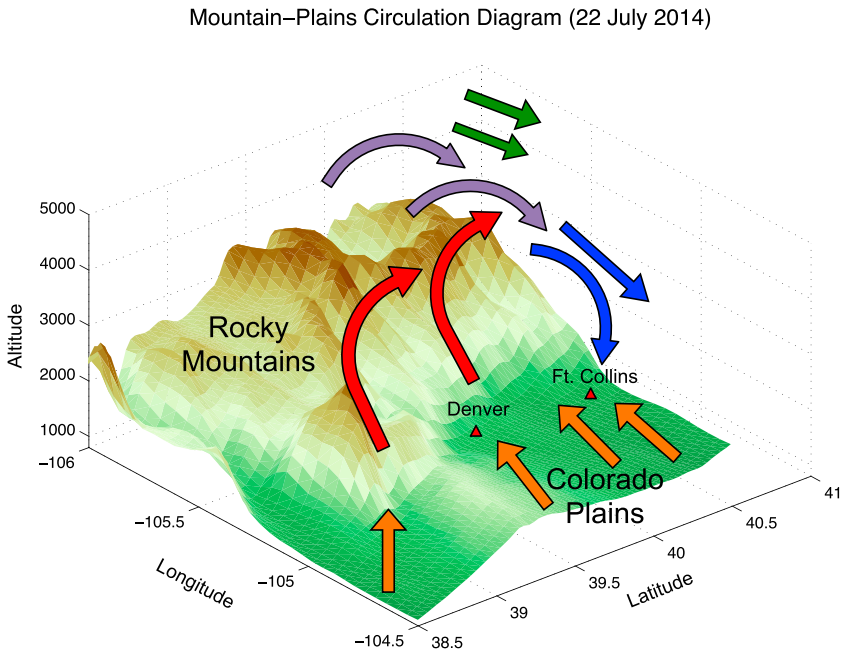

Figure 1. Differential insolation and thermal gradients between the Rocky Mountains and the Colorado Plains create daytime upslope flow that draws air from the plains toward the eastern ridge of the Rocky Mountains (orange arrows). This flow transports O_3 and other pollutants from the Front Range urban corridor and adjacent plains toward the foothills where they accumulate (red arrows) to higher elevations along the eastern slopes of the Rocky Mountains. The elevated flow (purple arrows) can interact with the weak synoptic winds (green arrows) and be recirculated back over the DNFR within the upper portion of a mountain-plains solenoid. The polluted air in the return flow aloft (blue arrow) can be carried eastward from the Front Range or can be mixed downward over the plains to further degrade the near-surface air quality.

This transport pattern is characterized by upslope (easterly) flow at lower levels, rising motion over the east side of the barrier (Rocky Mountains), westerly flow aloft, and sinking motion east of solenoid center. The solenoid axis is parallel to the mountain axis and is typically somewhere between the foothills and the plains. This system begins when differential insolation and thermal gradients between the Rocky Mountains and the Colorado Plains create daytime upslope flow that draws air from the plains toward the valley walls of the eastern ridges of the Rocky Mountains (orange arrows, Figure 1). This flow transports O_3 and other pollutants from the Front Range urban corridor and adjacent plains toward the foothills where they accumulate, with some of the polluted air transported further westward (red arrows, Figure 1) to higher elevations along the eastern slopes of the Rocky Mountains [e.g., *Parrish et al.*, 1986]. When the upslope flow is particularly strong, O_3 and other long-lived pollutants can be transported westward over the Continental Divide [*Bossert and Cotton*, 1994a, 1994b]. After sunset, the flow reverses and nocturnal drainage flows carry polluted air eastward (downsloping) along the South Platte River drainage into the western High Plains.

During the afternoon, the upslope flow along the surface interacts with the weak westerly synoptic winds (green arrows, Figure 1) in a leeside convergence zone near the Divide. The air mass is then lifted and recirculated back over the DNFR within the upper portion of a mountain-plains solenoid (purple arrows, Figure 1) [*Reiter and Tang*, 1984; *Wolyn and Mckee*, 1994; Zardi and Whiteman, 2013]. This phenomenon is akin to the "mountain chimney effect" observed in the Lower Fraser Valley, British Columbia [*McKendry et al.*, 1997] and the Los Angeles Basin [*Langford et al.*, 2010a]. This transport phenomenon was observed by airborne O_3 lidar during the 2008 Front Range Air Quality study [*Banta et al.*, 2013]. The polluted air in the return flow aloft (blue arrows, Figure 1) can be carried eastward from the Front Range or can be mixed downward over the plains to degrade near-surface air quality. Furthermore, based on this flow pattern, pollutants that vertically mix down via the mountain-plains solenoid have likely originated earlier in the day within the DNFR, suggesting that it is important to assess the full history and vertical extent of the polluted air.

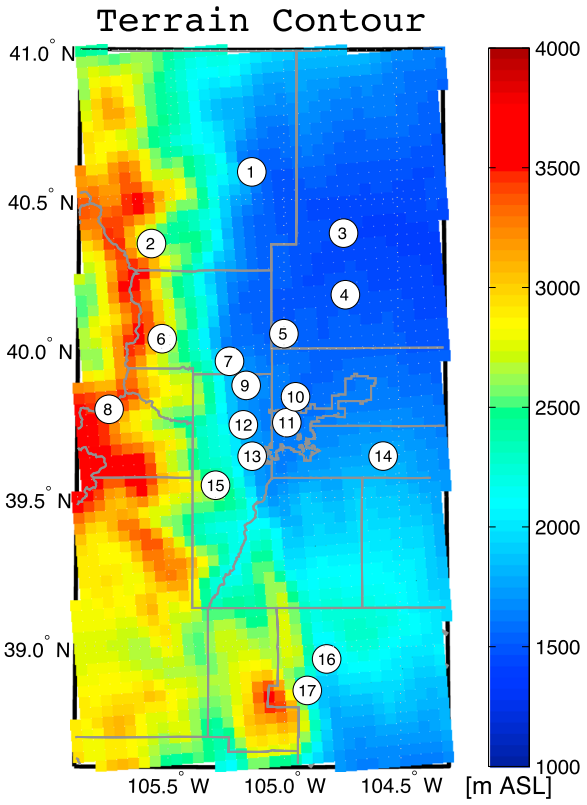

No.	Site	Name	Lat .	Lon	Elev. (m)	MDA8
1	**Ft. Collins - West**	FTCW	40.6	-105.1	1762.7	**76**
2	**Rocky Mtn NP**	RMNP	40.4	-105.6	2909.0	69
3	**Greeley Weld Twr**	GRET	40.4	-104.7	1431.1	60
4	Platteville	PTV	40.2	-104.7	1516.0	59
5	Boulder Atm. Obs.	BAO	40.1	-105.0	1584.0	**75**
6	Niwot Ridge (C-1)	NR	40.0	-105.5	3035.0	68
7	**S. Boulder Creek**	SBC	40.0	-105.2	1859.2	**75**
8	Mine's Peak	MP	39.8	-105.8	2850.0	70
9	**Rocky Flats - N**	RFN	39.9	-105.2	1744.1	**82**
10	**Welby**	WBY	39.8	-104.9	1592.4	67
11	**CAMP**	CAMP	39.8	-105.0	1612.8	59
12	**NREL-Golden**	NREL	39.7	-105.2	1832.2	**79**
13	**Chatfield Park**	WCH	39.6	-105.1	1859.1	**75**
14	**Aurora East**	AURE	39.6	-104.6	1819.8	58
15	**Aspen Park**	ASP	39.5	-105.3	2579.5	69
16	**USAF Acad.**	ACAD	39.0	-104.8	1992.4	61
17	**Manitou Spgs**	MAN	38.9	-104.9	2571.0	60

Figure 2. A terrain map and full list of monitoring locations for this study, which are mostly preestablished Colorado Department of Public Health and Environment (CDPHE) sites (http://www.colorado.gov/airquality). Regulatory monitors are shown in boldface. Their abbreviations, locations, elevations, and daily O_3 8 h average maxima are shown for 22 July 2014, where red denotes an exceedance of the 75 ppbv standard and orange denotes an exceedance of the new 70 ppbv standard.

In this paper, we describe an example of a recirculation episode that occurred on 22 July 2014 during the concurrent NASA 2014 "Deriving Information on Surface Conditions from Column and Vertically Resolved Observations Relevant to Air Quality" (DISCOVER-AQ) and "Front Range Air Pollution and Photochemistry Experiment" (FRAPPE) campaigns [*Crawford and Pickering*, 2014; *Pickering et al*., 2014]. We characterize the history of the polluted return air mass with a three-dimensional (horizontal, vertical, and temporal) view of O_3 throughout the full depth of the mountain-plains circulation within the DNFR obtained from continuous lidar observations in conjunction with radar wind profiles. We combine these observations with ancillary measurements from a network of surface monitors (Figure 2), the NASA P-3B, and balloon-borne instruments. Furthermore, air quality simulations and back trajectory analyses are employed to investigate the impacts of the recirculation on the high O_3 event that developed.

2. Meteorology

The second half of July 2014 was much wetter than normal along the Front Range with Boulder recording the fifth wettest July in 121 years of records [https://www.ncdc.noaa.gov/sotc/national/201407]. Frequent late afternoon thunderstorms disrupted the normal diurnal flow patterns and limited the accumulation of O_3 near the surface [*Langford et al*., 2010b]. As a result, there were only seven exceedances of the 2008 NAAQS of 75 ppbv at regulatory monitors in Colorado during July 2014 compared to 44 in July 2013 and 61 in July 2012 [http://www.airnow.gov]. These numbers would have been 24, 118, and 137, respectively, under the 2015 NAAQS of 70 ppbv. The three sites that violated the 2008 NAAQS on 22 July were Fort Collins-West (FTCW, circle 1 in Figure 2), Golden-National Renewable Energy Laboratory (NREL, circle 12 in Figure 2), and Rocky Flats North (RFN, circle 9 in Figure 2).

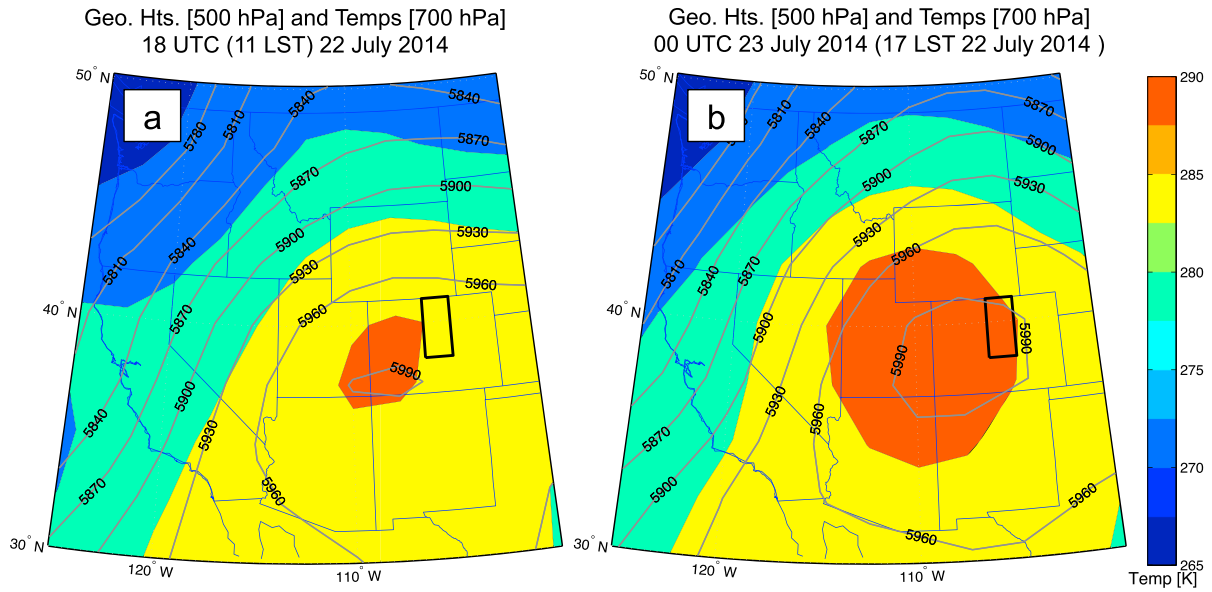

Figure 3. NCEP Reanalysis 500 hPa geopotential heights (meters above sea level) and 700 hPa temperatures (K) for (a) 1800 UTC 22 July 2014 and (b) 0000 UTC 23 July 2014. The domain region from Figure 1 is indicated in the black box.

The reanalysis (Figure 3a) at 1800 UTC (1100 local standard time, LST) on 22 July 2014, provided by the National Centers for Environmental Prediction/National Center for Atmospheric Research (NCEP/NCAR) [*Kalnay et al*., 1996], shows a strong anticyclonic system centered near the Four Corners region (i.e., the area where the states of Arizona, New Mexico, Utah, and Colorado meet) at 500 hPa and warmer temperatures at 700 hPa over the southern portion of the Rocky Mountain region. Figure 3b indicates that by 0000 UTC 23 July 2014, the upper level ridge had moved directly over the DNFR. The upper level ridge also exhibits strengthening indicated by warmer/subsiding air at 700 hPa and higher 500 hPa heights. In the Rocky Mountain region, upper level ridges are strongly correlated with higher MDA8 concentrations [*Reddy and Pfister*, 2016] in part because they reduce the synoptic flow at the surface and aloft and allow cyclic terrain-driven circulations to dominate, thereby reducing transport away from sources [*Riehl and Herkhof*, 1972].

3. Ozone and Wind Analyses

3.1. Surface Observations

The one-minute (1 min) (Figure 4a) and one-hour (1 h) (Figure 4b) O_3 time series from NREL, RFN, and FTCW on 22 July 2014 indicate similar concentrations at all three sites prior to 1800 UTC (1100 LST). The surface wind directions (Figure 4d) denote a distinct transition from northwesterly to northeasterly by 0700 LST at both the NREL and RFN sites, suggesting that upslope flow effects were largely established in the southern portion of the domain by this time. However, it is not until 0900 LST that surface winds transition to mostly northeasterly/southeasterly at the FTCW site. Regardless of flow direction prior to 1100 LST, the NREL site's proximity to the Denver metropolitan area leads to nearly 2–3 times as much fresh nitrogen dioxide (NO_2) emissions (Figure 4c) than at FTCW site, which is important because NO_2 is an O_3 precursor and a source of photochemical O_3 production.

Beginning around 1100 LST, the NREL site observes a peak in NO_2 emissions near 12–13 ppbv and is followed by a shift in wind direction toward southerly/southwesterly until 1400 LST. This is quickly followed at the NREL site by a rapid increase in O_3 to over 90 ppbv and a subsequent depletion of NO_2 to down near 5 ppbv. During this same time, the FTCW site has generally northeasterly flow associated with NO_2 values near 1–2 ppbv. However, the FTCW site observes O_3 values that are 10–30 ppbv less than the NREL site, indicating that the disparity in NO_2 concentration and timing of O_3 production, accumulation, and advection between the sites were significant during this time.

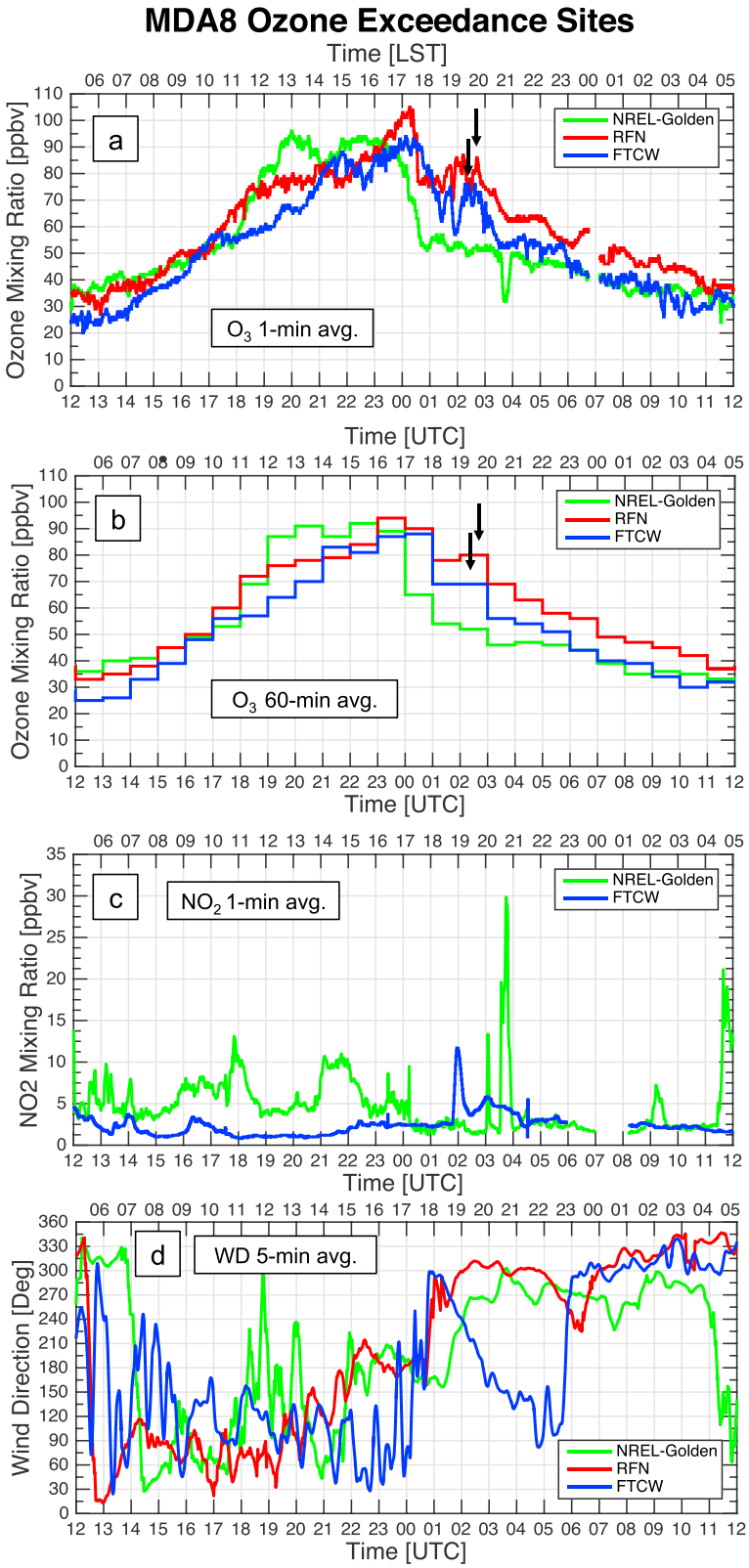

Figure 4. Time series of (a) 1 min O_3, (b) 1 h O_3, (c) 1 min NO_2, and (d) 5 min (1 min with a five-point smoothing applied) wind directions for the three sites that exceeded the NAAQS 75 eight-hour O_3 standard for 22 July 2014. NO_2 was unavailable at the RFN site during this time. The black arrows in Figures 4a and 4b indicate secondary maxima in O_3 at the RFN and FTCW sites.

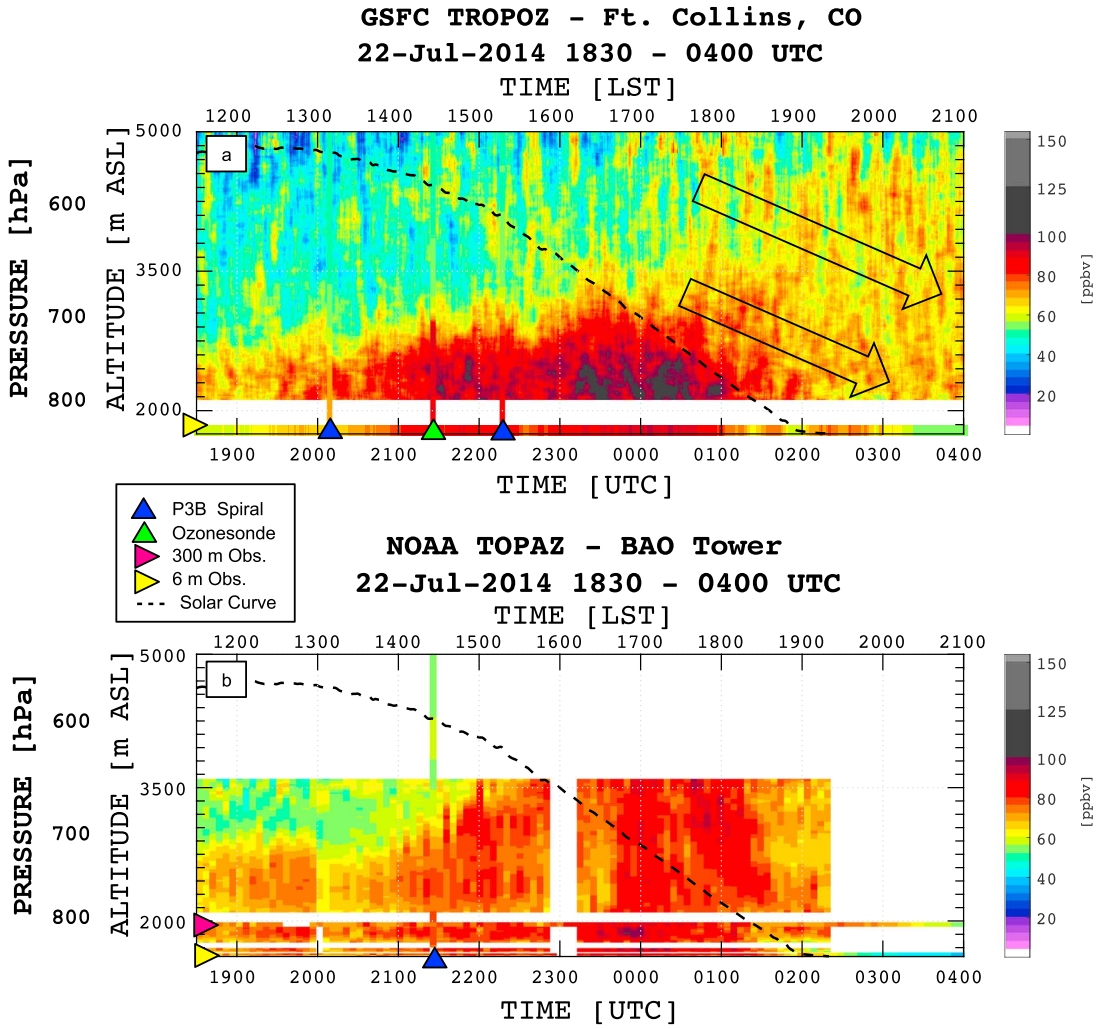

Figure 5. A time series of O_3 profiles during the DISCOVER-AQ/FRAPPE missions from 1830 UTC 22 July 2014 to 0400 UTC 23 July 2014 is shown for the (a) TROPOZ at the FTCW site and for the (b) TOPAZ at the BAO Tower site. The lidar profiles are reported at 5 min temporal resolution. The sonde profile at the FTCW site is denoted with the green triangle. The 1 min surface O_3 concentrations at 6 m agl are presented in the lowest data bin of each panel and are represented with the yellow triangle. An O_3 monitor sampling at 300 m agl was located at the BAO Tower and is denoted with a magenta triangle on the TOPAZ time series. Measurements of the solar radiation curve at FTCW are normalized in both panels.

As the winds at the NREL site return to easterly/northeasterly (from downtown Denver) from 1400 to 1500 LST, a secondary plume with similar NO_2 concentrations (as the first near 1100 LST) reaches the NREL site. This results in another perturbation in O_3 reaching values of 90 ppbv from 1500 to 1700 LST. Finally, a shift in winds at the NREL site to southerly after 1700 LST leads to a significant reduction in both NO_2 and O_3, resulting in observations below mostly 4 ppbv and 60 ppbv, respectively. This suggests that the NREL "early" peak in O_3 concentrations was influenced more by photochemical production with local precursors, while the decay in NREL O_3 was due to cleaning out with generally less polluted southerly flow that likely contained minimal solenoid return flow. The RFN site lies nearly due north of NREL (see Figure 2) and as the observed flow at NREL becomes predominantly southerly after 1700 LST, there is a rapid influx of O_3 (over 105 ppbv near 1715 LST) observed at the RFN site. To a lesser extent (likely due to the greater distance), a similar flow pattern impacted the FTCW monitor, which observed O_3 values over 90 ppbv. Although both the O_3 maxima observed at NREL were linked to increases in NO_2 emissions, the peak O_3 at the FTCW site occurred under the absence of change in NO_2 emissions, suggesting that transport is likely influencing the site more than photochemical production after 1500 LST.

Near 1730 LST, an abrupt change in the winds toward a westerly direction occurs at the RFN and FTCW sites, whereas the NREL site remains under southerly flow. Associated with this change at the RFN and FTCW sites

are initial 20–30 ppbv decreases in O_3, followed by O_3 concentrations near 65–85 ppbv from 1830 to 2000 LST. The sudden wind shifts, coupled with the delayed onset in oscillating levels of O_3, suggest induced turbulent vertical mixing of O_3 toward the surface during this time. Near 1900 LST, peak concentrations in NO_2 near 12 ppbv are observed, indicating that the mixing down and transport of additional precursors from surface sources occurred. A 30 ppbv spike in NO_2 occurs at the NREL site via drainage winds near 2100 LST, suggesting that chemical transport via return downsloping flow near NREL was more strongly composed of NO_2 and other O_3 precursors rather than O_3.

These secondary peaks in O_3, under the reduced solar radiation near sunset, indicate that direct local photochemical production was likely not solely responsible for the increase in O_3. Observations and simulations of recirculation aloft, vertical mixing, and downward transport on the eastern side of the mountain-plains solenoid will be critical in quantifying the air quality impacts at the RFN and FTCW sites. Because observed pollution levels were out of compliance with current regulatory standards, further wind and O_3 profiles, model simulations, and trajectory analyses will be used to evaluate the differences between the sites

3.2. Ozone Lidar Observations

Ozone lidar observations from the Tropospheric Ozone Lidar Network (TOLNet, http://www-air.larc.nasa.gov/missions/TOLNet) are used to characterize the O_3 vertical structure throughout 22 July 2014. Nearly continuous profiles of tropospheric O_3 were provided by the Goddard Space Flight Center Tropospheric Ozone Differential Absorption Lidar (GSFC TROPOZ DIAL [*Sullivan et al*., 2014]) deployed to the FTCW site (Figure 5a) and the NOAA Tunable Optical Profiler for Aerosols and oZone (TOPAZ) [*Alvarez et al*., 2011] deployed to the Boulder Atmospheric Observatory (BAO) tower site (Figure 5b). The different vertical ranges in Figure 5 reflect the different hardware configurations of the TOPAZ and TROPOZ systems. Both systems derive O_3 concentrations to within 10–15% compared to nearby sonde profiles [*Langford et al*., 2011; *Sullivan et al*., 2015]. The lidar measurements are augmented by in situ measurements from the NASA P-3B aircraft, which performed multiple spiral ascents and descents over several ground sites during the 2014 DISCOVER-AQ and FRAPPE campaigns. These profiles are overlaid on each of the lidar time series. An O_3-sonde, which was conditioned and prepared with current community standard practices [*Thompson et al*., 2007], was launched at 2130 UTC at the FTCW site. An in situ O_3 surface monitor at both sites (FTCW was previously shown in Figure 4) and a 300 m monitor at the BAO Tower site [*McClure-Begley et al*., 2015] are also overlaid on each time series.

From 2100 UTC to 0200 UTC (1400 to 1900 LST), increases in O_3 of 10–30 ppbv as compared to the concentrations prior to 2100 UTC were observed at both sites, with mixing ratios in excess of 90 ppbv at the BAO and 100 ppbv at FTCW. The TROPOZ, TOPAZ, O_3-sonde, and aircraft observations throughout the mixed layer are generally 10 to 20 ppbv higher than the surface monitors, indicating the importance of the vertical distribution of pollutants. The mixing heights at FTCW, defined by the largest O_3 gradient, are at 2.7 km above sea level (asl), 2.9 km asl, and 3.3 km asl, respectively, at 2010 UTC, 2130 UTC, and 2220 UTC. The TROPOZ measurements, which have previously used O_3 gradients to determine mixing heights [*Dreessen et al*., 2016], show a well-defined O_3 gradient between defining the top of the mixed layer from 2.5–3.4 km asl throughout the day, which compares well with the aircraft and sonde. The TROPOZ observations indicate that the O_3 mixing height continued to grow throughout the day, even as solar radiation began to diminish, indicating that O_3 mixing likely persisted throughout the evening hours. Another O_3-sonde launched at 2045 UTC from the Platteville site nearly 50 km to the southeast of FTCW (cf. Figure 1) showed a mixed layer with 70 ppbv of O_3 from the surface to nearly 3.1 km asl. The mixed layer was also slightly deeper at the BAO and grew beyond the range of TOPAZ in the late afternoon, consistent with the 3.7 km asl mixed layer depth from the 00 UTC (17 LST) sounding from Denver International Airport, which is located nearly 35 km SE of the BAO.

After 0100 UTC, TROPOZ observations indicate persistent levels of enhanced O_3 aloft between 2000 and 5000 m asl (illustrated with arrows and increase in surface O_3). O_3-rich air (65–85 ppbv) appears below and above the mountaintop height (heights shown in Figures 1 and 2) and persists throughout the remainder of the observation period (to 0400 UTC 23 July 2014). The increased concentrations of O_3 aloft, coupled with the timing of the secondary maximum in the surface concentrations at RFN and FTCW, suggest that downward mixing of O_3 pushed concentrations at the FTCW site (and the RFN site) above the regulatory standard.

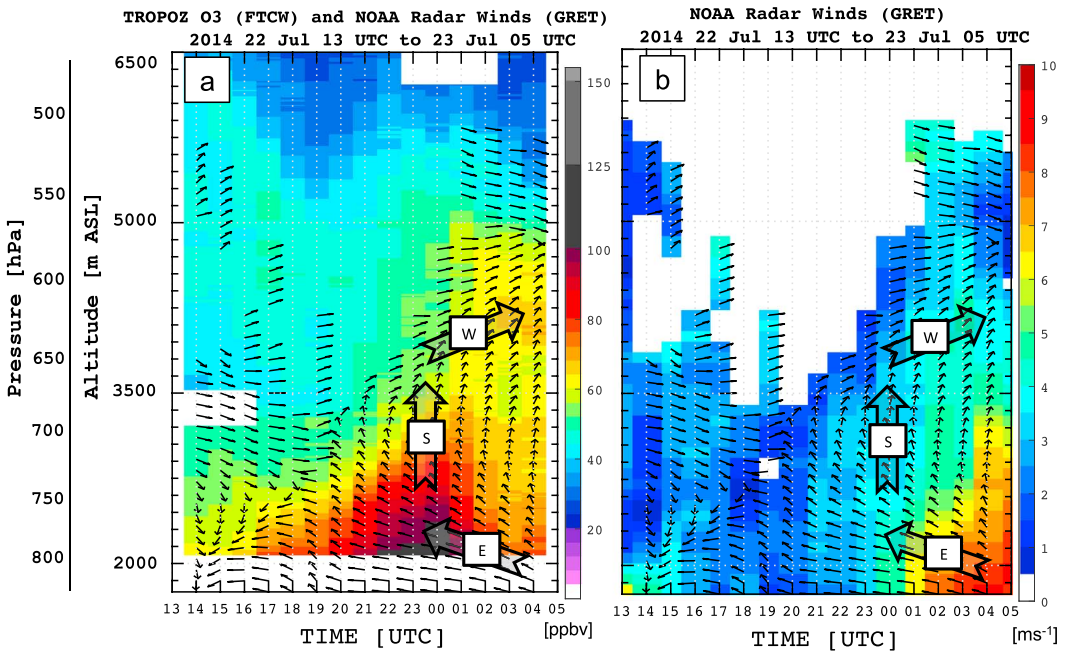

Figure 6. Composite hourly profiles of (a) O_3 and wind direction and (b) wind speed and direction from the TROPOZ (FTCW) and NOAA wind profiler (GRET) during the DISCOVER-AQ/FRAPPE campaigns from 1300 UTC 22 July 2014 to 0500 UTC 23 July 2014. The pressure scale is shown for comparisons to model simulations.

3.3. Composite Ozone-Wind Profiles

To better understand the transport and dynamics of O_3 throughout the domain and its impacts on air quality, a composite figure of the TROPOZ O_3 observations and horizontal wind directions (Figure 6a) and speeds (Figure 6b) from the NOAA Greeley (GRET, circle 3 in Figure 2) 915 MHz radar wind profiler are shown from 1300 to 0500 UTC (0600–2200 LST). After 1500 UTC, the wind profiles reveal an easterly mean flow at 800 hPa (near 2000 m asl), indicating thermally driven upslope flow and persistent 1–3 m s^{-1} easterly/southeasterly winds thereafter. During this time, pollutants are pulled from the Colorado Plains toward the foothills of the Rocky Mountains (see orange arrows in Figure 1). A directional wind shear between the lower level easterly flow and westerly flow aloft helps to define the ozone mixing height throughout the day.

Between 2000 and 0100 UTC, the mean large-scale flow increases to 3–5 m s^{-1} at 700 hPa (near 3200 m asl) and has a southerly component which flows along the mountain axis throughout the DNFR (see red arrows in Figure 1). Furthermore, the background westerly synoptic winds were generally between 2 and 4 m s^{-1} throughout the high O_3 event, indicating that thermal flows developed under relatively quiescent synoptic conditions. TROPOZ observations indicate that the peak boundary layer O_3 from 2200 to 0100 UTC corresponds to southeasterly flow, further indicating transport as the source of enhanced levels of pollutants. Near 2200 UTC, vertical wind shear (in direction and speed) exists between the background westerlies/southwesterlies at 650 hPa (near 3800 m asl, see green arrows in Figure 1) and the southerly flow at 700 hPa (near 3200 m asl, see purple arrows in Figure 1), which is an important mechanism for turbulent mixing and transport between vertical layers [*Horst and Doran*, 1988]. After this vertical mixing, the flow in the 700 hPa layer at 0100 UTC corresponds to O_3 concentrations of 10–20 ppbv higher compared to this altitude at 1800 UTC, and O_3 continues to persist as a reservoir aloft for the remainder of the observations at 0400 UTC (see blue arrows in Figure 1). Importantly, the lidar measurements of high O_3 aloft corresponding to westerly flow, particularly at and above the mountaintop height, are a direct evidence of an established mountain-plains circulation.

4. Simulations and Discussion

4.1. U.S. EPA Community Multiscale Air Quality Ozone Simulation

To evaluate the spatial distribution and chemical transport of O_3 on 22 July 2014, experimental forecasts of O_3 (Figures 7a–7c) and vertical winds (Figures 7d–7f) from the U.S. EPA Community Multiscale Air Quality

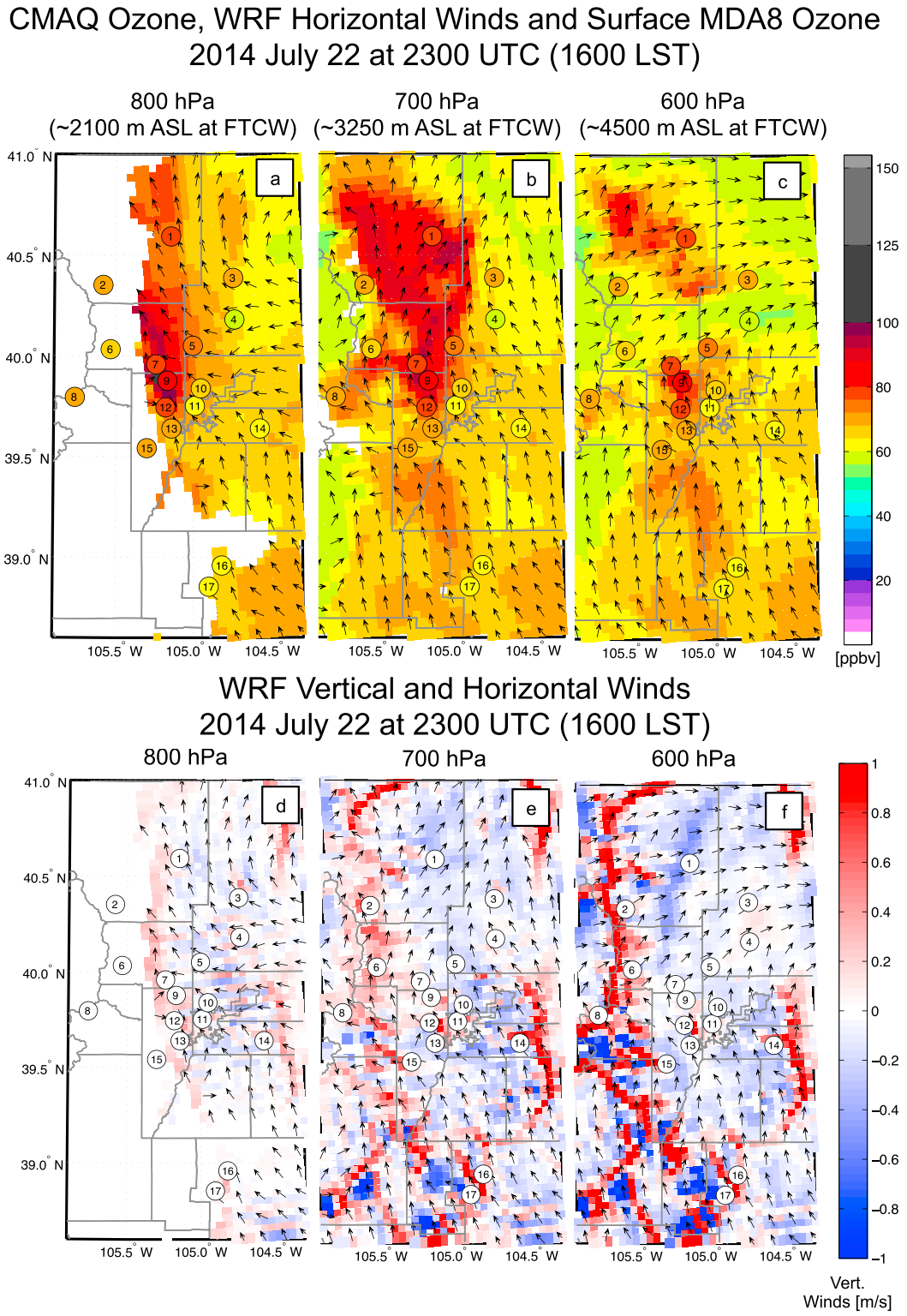

Figure 7. CMAQ model hourly output of O_3 and WRF-ARW vertical winds on 22 July 2014 at 2300 UTC (1600 LST) in the layers corresponding to (a and d) 800 hPa, (b and e) 700 hPa, and (c and f) 600 hPa. The horizontal WRF-ARW wind directions are overlaid on each panel. The MDA8 O_3 value (shown as color within the site number circles in Figure 2) from each surface-monitoring site is also overlaid on Figures 7a–7c.

(CMAQ v. 4.7.1.) model [*Lee and Ngan*, 2011; *Tang et al*., 2016] are presented. The chemical mechanisms in the model runs, performed by the NOAA Air Resource Laboratory (ARL), are driven offline with meteorological input from the Weather Research and Forecasting Advanced Research (WRF-ARW) mesoscale numerical weather prediction system with a $4 \times 4\,km^2$ horizontal grid spacing. The meteorological WRF model and CMAQ share the same sigma-p vertical structure with 42 unevenly spaced layers [*Appel et al*., 2007]. The first layer was 8 m above ground level (agl), and the lowest 2 km was modeled by 15 layers with finer grid spacing in the lower layers. The simulations are presented at 2300 UTC (1600 LST) corresponding to the time when the O_3 lidar and radar wind observations (Figure 6) indicate establishment of the mountain-plains recirculation. This time also coincides with the peak surface O_3 exceedance at the NREL site (Figure 4).

At 800 hPa (Figures 7a and 7d), CMAQ peak O_3 concentrations are between 80 and 100 ppbv and are mostly centered around the Denver metropolitan area stretching northward to the FTCW site. Sites that are closest to the eastern ridge of the Rocky Mountains are generally more polluted than those throughout the plains, which is a result of persistent easterly upslope flow in the near-surface layers including 800 hPa (see Figure 7d) and the interactions between transport and photochemistry during the period. Although there is some uncertainty in the O_3 sources, O_3 precursor emissions from the DNFR region likely were transported from the Platte Valley where emissions accumulate in the early morning via valley drainage and slope flows [*Reddy and Pfister*, 2016].

The 700 hPa level (Figures 7b and 7e) lies near the height of the Continental Divide, and the CMAQ simulation is representative of the mean O_3 throughout the PBL for most of the sites throughout the DNFR. The high-O_3 plume (as compared to the 800 hPa layer) has expanded much further eastward into the DNFR, due to the mean southerly and southwesterly winds and downward transport within the solenoid circulation. The simulation suggests that the increased O_3 observed at sites in the southern portion of the domain is rising and moving toward the northern portion of the domain via mountain-plains solenoid flow. By this time, increased O_3 concentrations associated with upslope flow have also affected observations at high-elevation sites (Figures 7b and 7e). In the DNFR, the peak measured concentrations impact the RFN (circle 9 in Figures 2 and 7), South Boulder Creek (SBC, circle 7 in Figures 2 and 7), and the NREL site (circle 12 in Figures 2 and 7). The high O_3 conditions stretch up toward the FTCW site (circle 1 in Figures 2 and 7) and the BAO (circle 5 in Figures 2 and 7) and are evident in both O_3 lidars (Figure 5). The high O_3 plume from Figure 7b coincides with subsidence on the eastern side of the Rocky Mountains, indicating that the O_3 plume was likely entrained within the solenoidal flow and was vertically advected toward the surface. The mean vertical wind speeds near the FTCW site are downward between 0.20 and 0.30 $m\,s^{-1}$ (720–1080 $m\,hr^{-1}$), which are more than adequate to bring the polluted air mass to the surface within 2–3 h.

At 600 hPa (Figures 7c and 7f), the CMAQ simulation reproduces a similar mean O_3 concentration as that from the TROPOZ throughout the region centered in the return flow aloft (see Figure 5). Westerly winds are more established over the northern portion of the domain, and the simulation indicates that the return flow contains high O_3 concentrations near the FTCW site and the Denver metropolitan region. Furthermore, the eastern portion of the high O_3 plume corresponds to a prominent region of strong subsidence, stretching from SBC (circle 7) to the northern portion of the domain. The mean downward vertical velocity in this region is between 0.40 and 0.50 $m\,s^{-1}$ (1440–1800 $m\,hr^{-1}$), which could also lead to vertical advection to the 700 hPa level within an hour and to the surface at the FTCW site within 2–3 h. CMAQ simulates rising motion over the higher terrain and sinking motion over the plains. Thus, it is evident that the presence of the solenoid circulation likely returned O_3 and its precursors back to sites within the DNFR. Specifically, the enhanced 600 hPa O_3 concentrations spatially coincide with the FTCW, NREL, and RFN sites, which recorded MDA8 values in exceedance of the 75 ppbv NAAQS. The BAO and SBC monitoring sites, which were 1 ppbv below the 2008 EPA NAAQS, also corresponded to the region aloft of higher O_3 concentrations.

4.2. CMAQ Surface Evaluation at MDA8 Exceedance Sites

The WRF/CMAQ simulations reproduce the regional air quality effects of the mountain-plains solenoid, and it is useful to compare the model output to surface observations for further regulatory interest (Figure 8). CMAQ captures the diurnal trends at each MDA8 site, indicating that peak O_3 occurred between 1200 and 1700 LST, and diminishing O_3 during nighttime hours. In the morning hours (0500 to 1000 LST), the simulation agrees

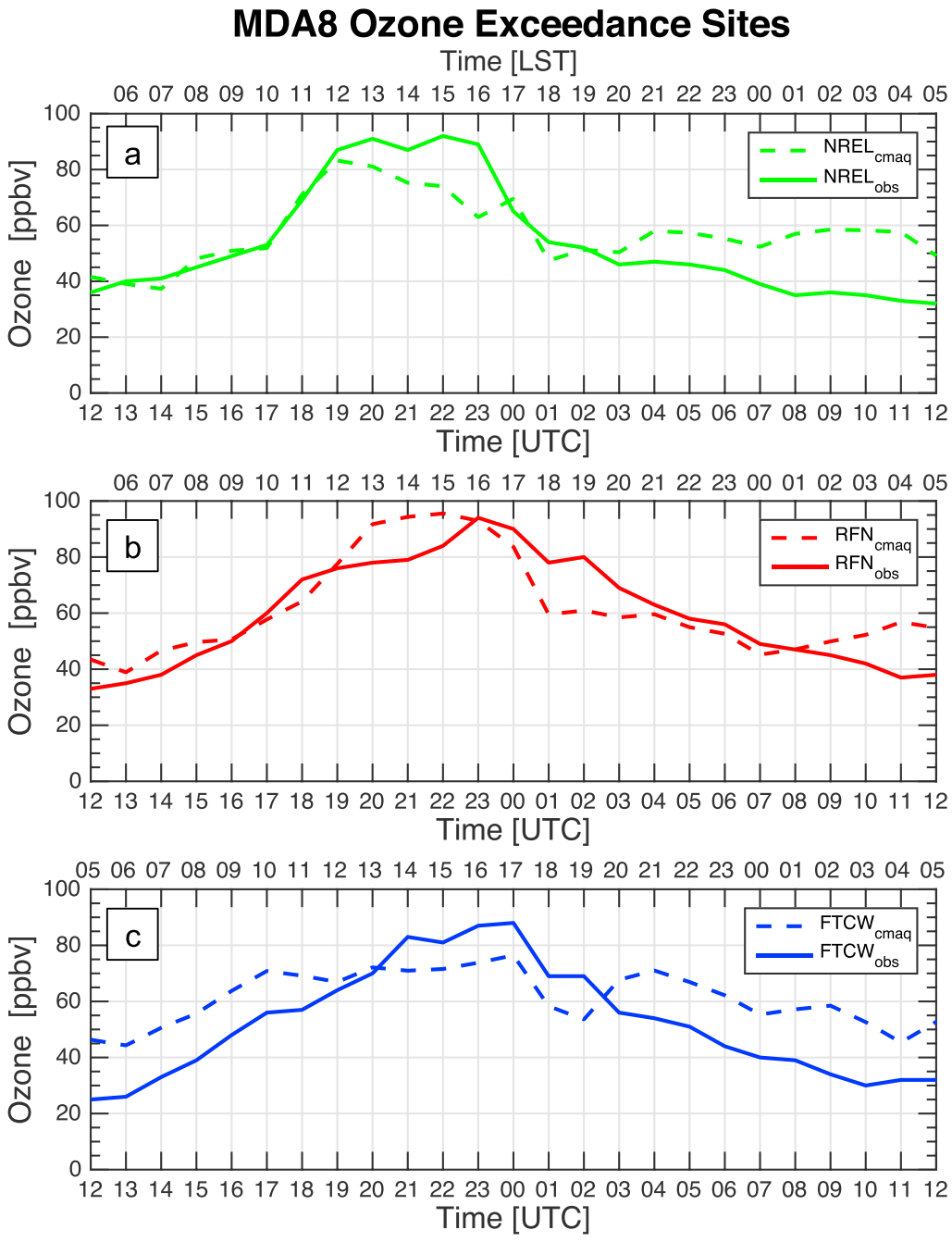

Figure 8. CMAQ evaluation for the three sites that exceeded the MDA8 O_3 standard: (a) NREL, (b) RFN, and (c) FTCW. The observations and model output are indicated with solid lines and dashed lines, respectively.

to within 5 ppb at the NREL and RFN sites, suggesting that the model is accurately simulating the nighttime and early morning chemistry [*Tang et al.*, 2016]. However, during these morning hours, the model largely overestimates O_3 concentrations at the FTCW site by 15–20 ppbv. Although during the morning hours at FTCW there is an overestimation in absolute concentration, the model generally matches the rate of O_3 production in the observations. At 1000 LST, the timing and rate of the initial rapid O_3 production is captured very well in the simulation at the NREL site. However, the model largely underestimates the persistence of the elevated O_3 observations above 80 ppbv until 1600 LST. At RFN the simulation produces O_3 too early, which results in an overestimation of 10–15 ppbv from 1300–1500 LST ppbv and an underestimation of nearly the same amount from 1700 to 2000 LST.

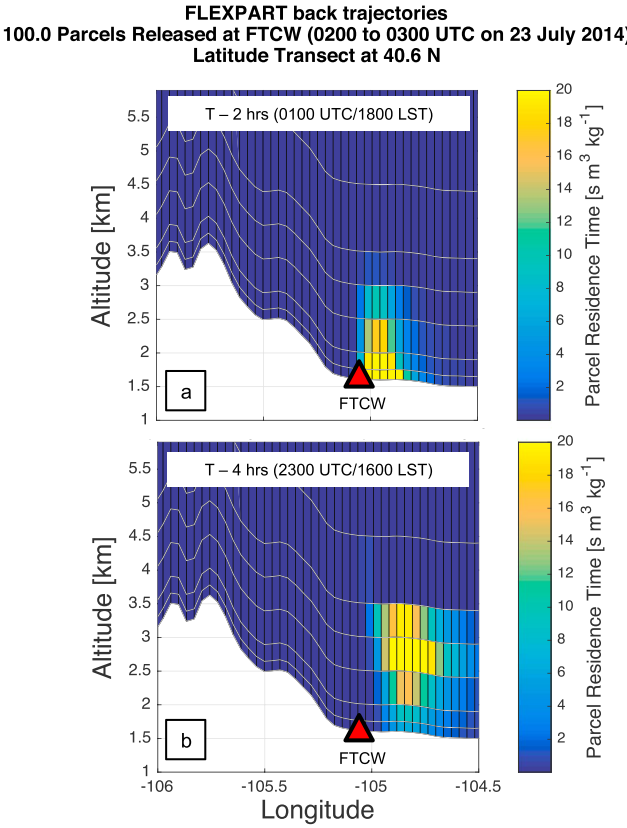

Figure 9. Vertical distribution of parcel concentration along 40.6 N (east-west through northern Colorado) output from the FLEXPART back trajectory calculation at (a) 0100 UTC (1800 LST) and (b) 2300 UTC (1600 LST 22 July 2014). One hundred parcels were released at the FTCW site between 0200 and 0300 UTC (2000 LST). Higher residence times indicate that more parcels spend more time in a grid cell.

Overall, CMAQ simulates the O_3 trends at the FTCW site from 1400 to 1900 LST; however, it is largely underestimating concentrations by 5–10 ppbv. Importantly, the simulation correctly indicates the timing of the peak O_3 at FTCW at 1700 LST and demonstrates the secondary maxima near 2100 LST. Although the secondary maxima are delayed with respect to the observations, the absolute concentration is within 2 ppbv of the observations. This reproduction in overall O_3 behavior at each site, as well as the secondary maxima of O_3 at the FTCW site, adds confidence to the model and suggests that it was correctly simulating regional effects of the mountain-plains solenoid.

4.3. FLEXPART Back Trajectory Analyses

The combination of high-resolution O_3 lidar observations (Figures 5 and 6) and CMAQ simulations (Figure 7) indicate peak O_3 concentrations near 100 ppbv throughout the first 2 km agl; however, the extent of vertical mixing has not been explicitly addressed. Back trajectory analyses (Figures 9a and 9b) are presented to illustrate the impact of vertical transport to the surface at the FTCW site at 0300 UTC (2000 LST), the closest model output to the secondary O_3 maxima observed (black arrows, Figure 3). The back trajectory calculations were performed using the Lagrangian particle dispersion model FLEXPART-WRF [http://flexpart.eu; *Brioude et al.*, 2013], driven by WRF-ARW meteorology at 3 km horizontal resolution, to understand the origin of the air mass sampled at FTCW. In such a simulation, thousands of "air parcels" are released (e.g., from the location of an instrument such as the TROPOZ O_3 lidar), and their trajectory is followed back in time. Chaotic processes like turbulence or convection are applied in a stochastic manner to each parcel. At regular time intervals (e.g., 1 h), the concentration of parcels in each cell of a regular grid is calculated. This provides a statistical estimate of the airmass location at this point in time and hence an estimate of the history of the airmass sampled at the instrument location. In our case, 100 parcels were released at the surface grid point (0–50 m agl) at FTCW between 0200 and 0300 UTC 23 July 2014 and followed back in time for 24 h.

The airmass location (Figure 9a) at 0100 UTC/1800 LST (2 h prior to the secondary surface maxima) indicates that a substantial portion of the air sampled at the surface originated from higher altitudes. The highest concentrations of parcel origins are mostly below 2.5 km asl on the eastern side of the Rocky Mountains. The airmass location (Figure 9b) at 2300 UTC/1600 LST (4 h prior to the secondary surface maxima) shows the highest parcel concentrations between 2.0 and 3.5 km asl, still on the eastern side of the Rocky Mountains. These results imply that the O_3 plume quantified with the lidar observations and CMAQ simulation mixed down to reach the surface at the FTCW site. The trajectories indicate that the largest concentrations of parcels originated east of the ground site, suggesting that during the entrainment of high O_3, persistent low-level easterly winds (cf. Figure 6) continued near the surface. This confirms

not only that the mountain-plains circulation was fully established but also that it was the meteorological mechanism responsible for recirculating high O_3 air to the surface within the DNFR during the evening hours on 22 July 2014.

5. Conclusions

The observations and simulations presented here describe an elevated O_3 pollution episode that occurred on 22 July 2014 during the DISCOVER-AQ and FRAPPE campaigns. Under relatively weak synoptic conditions, convective upslope flow and the mountain-plains solenoid circulation were established and subsequently exacerbated O_3 concentrations in the Colorado Front Range. The combination of high-resolution O_3 measurements, chemical simulations, and back trajectories indicate that this complex flow pattern caused the Fort Collins-West, NREL-Golden, and Rocky Flats North sites to exceed the 2008 75 ppbv NAAQS. Although the RFN site was largely above the standard on this day, if the FTCW site had not received the secondary increase in O_3 (i.e., 1 h values 3–4 ppbv less than observed at 0200 UTC), it would have remained below the 75 ppbv NAAQS. Furthermore, with the 2015 (70 ppbv) regulations in place, three additional sites would have been above the standard on this day, and total exceedances at regulatory monitoring sites throughout Colorado would have increased from 24 to 44 in July 2014, 44 to 118 in July 2013, and 61 to 137 in July 2012 [http://www.airnow.gov]. Because of these increasingly stringent regulatory criteria, it is critical to analyze the vertical characteristics of terrain-induced O_3 episodes in regions that are already at or near nonattainment status [*EPA*, 2015b; *Cooper et al*., 2015]. Another mesocale circulation pattern, the Denver Cyclone, also occurred during the concurrent campaigns, indicating that the complex meteorology in this region can significantly exacerbate pollution levels [*Vu et al*., 2016]. As we have shown, high-resolution vertical profiles of O_3 from multiple TOLNet O_3 lidars, in conjunction with model simulations, have added valuable insight into the quantification of a policy-relevant air quality event in a complex region.

Acknowledgments

Unless otherwise noted, all data used in this study can be found in the DISCOVER-AQ data archive (http://www-air.larc.nasa.gov/missions/discover-aq/), the FRAPPE data archive (http://catalog.eol.ucar.edu/frappe), or the TOLNet data archive (http://www-air.larc.nasa.gov/missions/TOLNet/). This work was supported by UMBC/JCET (task 374, project 8306), the Maryland Department of the Environment (MDE, contract U00P4400079), and NOAA-CREST CCNY Foundation (subcontract 49173B-02). This research was supported by an appointment to the NASA/USRA Postdoctoral Program at the Goddard Space Flight Center. The Platteville Nittany Atmospheric Trailer and Integrated Validation Experiment (NATIVE) operations were sponsored by NASA DISCOVER-AQ grant NNX10AR39G and the Pennsylvania State University. The authors gratefully acknowledge support provided by the NASA Tropospheric Chemistry Program and the Tropospheric Ozone Lidar Network (TOLNet). Thanks to the helpfulness and expertise of Ryan Stauffer, Hannah Halliday, and Nikolai Balashov, who worked with the NATIVE trailer at Platteville. Thanks to Debra Wicks Kollonige for providing her insight and recommendations on this work. Thanks to Kenneth Pickering, Yonhua Tang, Li Pan, and Barry Baker for their expertise in evaluating and managing the CMAQ model output. Thanks to Timothy Coleman (NOAA ESRL PSD) for providing the Greeley wind profiles. Thanks to the NOAA Physical Science Division for their continued efforts in managing the instrumentation and site coordination necessary for this work from the 300 m BAO Tower. Finally, thanks to the CDPHE for the continued efforts to obtain observations at the many remote and urban sites throughout the region used in this work. The views, opinions, and findings contained in this report are those of the author(s) and should not be construed as an official National Oceanic and Atmospheric Administration or U.S. Government position, policy, or decision.

References

Alvarez, R. J., et al. (2011), Development and application of a compact, tunable, solid-state airborne O_3 lidar system for boundary layer profiling, *J. Atmos. Oceanic Technol.*, *28*(10), 1258–1272.

Appel, K. W., A. B. Gilliland, G. Sarwar, and R. C. Gilliam (2007), Evaluation of the Community Multiscale Air Quality (CMAQ) model version 4.5: Sensitivities impacting model performance: Part I—O_3, *Atmos. Environ.*, *41*(40), 9603–9615.

Banta, R. M., C. M. Shun, D. C. Law, W. Brown, R. F. Reinking, R. M. Hardesty, C. J. Senff, W. A. Brewer, M. J. Post, and L. S. Darby (2013), Observational techniques: Sampling the mountain atmosphere, in *Mountain Weather Research and Forecasting*, edited by F. K. Chow, S. F. J. De Wekker, and B. J. Snyder, pp. 409–530, Springer, Netherlands.

Benedict, K. B., D. Day, F. M. Schwandner, S. M. Kreidenweis, B. Schichtel, W. C. Malm, and J. L. Collett (2013), Observations of atmospheric reactive nitrogen species in Rocky Mountain National Park and across northern Colorado, *Atmos. Environ.*, *64*, 66–76.

Bossert, J. E., and W. R. Cotton (1994a), Regional-scale flows in mountainous terrain. Part I: A numerical and observational comparison, *Mon. Weather Rev.*, *122*(7), 1449–1471.

Bossert, J. E., and W. R. Cotton (1994b), Regional-scale flows in mountainous terrain. Part II: Simplified numerical experiments, *Mon. Weather Rev.*, *122*(7), 1472–1489.

Brioude, J., et al. (2013), The Lagrangian particle dispersion model FLEXPART-WRF version 3.1, *Geosci. Model Dev.*, *6*(6), 1889–1904.

Cooper, O. R., A. O. Langford, D. D. Parrish, and D. W. Fahey (2015), Challenges of a lowered US O_3 standard, *Science*, *348*(6239), 1096–1097.

Crawford, J. H., and K. E. Pickering (2014), *DISCOVER-AQ: Advancing Strategies for Air Quality Observations in the Next Decade, EM Magazine*, pp. 4–7, Air & Waste Management Association, Pittsburgh, Pa.

Dreessen, J., J. T. Sullivan, and R. Delgado (2016), Observations and impacts of transported Canadian wildfire smoke on ozone and aerosol air quality in the Maryland region on 9–12 June, 2015, *J. Air Waste Manage. Assoc.*, doi:10.1080/10962247.2016.1161674.

U.S. Environmental Protection Agency (EPA) (2015a), Implementing the 2015 O_3 National Ambient Air Quality Standards, Accessed 1 December 2015. [Available online at http://www3.epa.gov/O3pollution/pdfs/20151001memo.pdf.]

U.S. Environmental Protection Agency (EPA) (2015b), Mandatory Class I areas, Accessed 1 December 2015. [Available online at http://www3.epa.gov/visibility/classimp.gif.]

Horst, T. W., and J. C. Doran (1988), The turbulence structure of nocturnal slope flow, *J. Atmos. Sci.*, *45*(4), 605–616.

Kalnay, E., et al. (1996), The NCEP/NCAR 40-year reanalysis project, *Bull. Am. Meteorol. Soc.*, *77*(3), 437–471.

Langford, A. O., C. J. Senff, R. J. Alvarez, R. M. Banta, and R. M. Hardesty (2010a), Long-range transport of ozone from the Los Angeles Basin: A case study, *Geophys. Res. Lett.*, *37*, L06807, doi:10.1029/2010GL042507.

Langford, A. O., S. C. Tucker, C. J. Senff, R. M. Banta, W. A. Brewer, R. J. Alvarez, R. M. Hardesty, B. M. Lerner, and E. J. Williams (2010b), Convective venting and surface ozone in Houston during TexAQS 2006, *J. Geophys. Res.*, *115*, D16305, doi:10.1029/2009JD013301.

Langford, A. O., C. J. Senff, R. J. Alvarez, R. M. Banta, R. M. Hardesty, D. D. Parrish, and T. B. Ryerson (2011), Comparison between the TOPAZ airborne O_3 lidar and in situ measurements during TexAQS 2006, *J. Atmos. Oceanic Technol.*, *28*(10), 1243–1257.

Lee, P., and F. Ngan (2011), Coupling of important physical processes in the planetary boundary layer between meteorological and chemistry models for regional to continental scale air quality forecasting: An overview, *Atmosphere*, *2*(3), 464–483.

McClure-Begley, A., I. Petropavlovskikh, and S. Oltmans (2015), NOAA Global Monitoring Surface Ozone Network, Accessed 1 December 2015, National Oceanic and Atmospheric Administration, Earth Systems Research Laboratory Global Monitoring Division. Boulder, Colo., doi:10.7289/V57P8WBF.

McKendry, I. M., D. G. Steyn, J. Lundgren, R. M. Hoff, W. Strapp, K. Anlauf, F. Froude, J. B. Martin, R. M. Banta, and L. D. Olivier (1997), Elevated ozone layers and vertical down-mixing over the Lower Fraser Valley, B. C, *Atmos. Environ.*, *31*, 2135–2146.

Parrish, D. D., D. W. Fahey, E. J. Williams, S. C. Liu, M. Trainer, P. C. Murphy, D. L. Albritton, and F. C. Fehsenfeld (1986), Background ozone and anthropogenic ozone enhancement at Niwot Ridge, Colorado, *J. Atmos. Chem.*, *4*, 63–80.

Pétron, G., et al. (2012), Hydrocarbon emissions characterization in the Colorado Front Range: A pilot study, *J. Geophys. Res. 117*, D04304, doi:10.1029/2011JD016360.

Pickering, K., J. Crawford, G. Pfister, and P. Lee (2014), The July–August DISCOVER-AQ and FRAPPE field campaigns in the front range region of Colorado: Summary of experiment design and preliminary findings, in 13th Annual Community Modeling and Analysis (CMAS) Conference.

Reddy, P. J., and G. G. Pfister (2016), Meteorological factors contributing to the interannual variability of mid-summer surface ozone in Colorado, Utah, and other western US states, *J. Geophys. Res. Atmos*, *121*, 2434–2456, doi:10.1002/2015JD023840.

Reiter, E. R., and M. Tang (1984), Plateau effects on diurnal circulation patterns, *Mon. Weather Rev.*, *112*(4), 638–651.

Riehl, H., and D. Herkhof (1972), Some aspects of Denver air pollution meteorology, *J. Appl. Meteorol.*, *11*(7), 1040–1047.

Sullivan, J. T., T. J. McGee, G. K. Sumnicht, L. W. Twigg, and R. M. Hoff (2014), A mobile differential absorption lidar to measure sub-hourly fluctuation of tropospheric O_3 profiles in the Baltimore–Washington, DC region, *Atmos. Meas. Tech.*, *7*(10), 3529–3548.

Sullivan, J. T., T. J. McGee, R. DeYoung, L. W. Twigg, G. K. Sumnicht, D. Pliutau, T. Knepp, and W. Carrion (2015), Results from the NASA GSFC and LaRC O_3 lidar intercomparison: New mobile tools for atmospheric research, *J. Atmos. Oceanic Technol.*, *32*(10), 1779–1795.

Tang, Y., L. Pan, P. Lee, D. Tong, H.-C. Kim, J. Wang, and S. Lu (2016), The performance and issues of a regional chemical transport model during Discover-AQ 2014 aircraft measurements over Colorado, in *Air Pollution Modeling and Its Application XXIV*, pp. 635–640, Springer International Publishing.

Thompson, A. M., J. C. Witte, H. G. J. Smit, S. J. Oltmans, B. J. Johnson, V. W. J. H. Kirchhoff, and F. J. Schmidlin (2007), Southern Hemisphere Additional O_3sondes (SHADOZ) 1998–2004 tropical O_3 climatology: 3. Instrumentation, station-to-station variability, and evaluation with simulated flight profiles, *J. Geophys. Res.*, *112*, 8241, doi:10.1029/2002JD002241.

Toth, J. J., and R. H. Johnson (1985), Summer surface flow characteristics over northeast Colorado, *Mon. Weather Rev.*, *113*(9), 1458–1469.

Vu, K. T., et al. (2016), Impacts of the Denver cyclone on regional air quality and aerosol formation in the Colorado Front Range during FRAPPÉ 2014, *Atmos. Chem. Phys. Discuss.*, doi:10.5194/acp-2016-532, in review.

Wolyn, P. G., and T. B. Mckee (1994), The mountain-plains circulation east of a 2-km-high north-south barrier, *Mon. Weather Rev.*, *122*(7), 1490–1508.

Zardi, D., and C. D. Whiteman (2013), Diurnal mountain wind systems, in *Mountain Weather Research and Forecasting*, pp. 35–119, Springer, Netherlands.